Printed Circuit Board Coils of Multi-track Litz Structure for 3.3 kW Inductive Power Transfer System

A. Narvaez, *Student Member, IEEE,* C. Carretero, *Senior Member, IEEE,* I. Lope, *Member, IEEE,* and J. Acero, *Senior Member, IEEE*

***Abstract*—This paper presents the optimization procedure of an inductive power transmission (IPT) system which utilizes large size spiral printed circuit board (PCB) coils for high-power transfer. Printed circuit boards (PCBs) for coil assembly provides advantages in the manufacturing process through the use of cost-effective flexible fabrication techniques. Furthermore, this kind of construction offers a low profile device, which is of great interest for applications with space constraints. PCB-based IPT system coils can achieve high energy efficiency by applying litz-structure braiding techniques, as investigated in this work, where the objective was to obtain an optimized balance between the conduction losses and proximity losses associated with the number and cross-section area of the traces. Considering the geometrical dimensions and manufacturing constraints, we will proceed to obtain the characteristics of the coil to achieve optimal performance. The estimation of coil losses were in part based on finite element simulations, and the results were conveniently processed with the appropriate mathematical methods. Numerical simulation and experimental results were conducted for validation on a prototype suitable to transfer up to 3.3 kW for a transmitter-receiver distance of 10 cm. In the experimental arrangement, a maximum efficiency in the coils of 93% has been measured, and the efficiency of 88% has been reached for the entire IPT system.**

***Index Terms*—Inductive power transfer system, wireless charging, wireless power transmission, printed circuit board coils.**

I. Introduction

NOWADAYS, energy efficiency is one of the most important issues in the development of all new generation systems due to a possible energy crisis. This is a key factor to take into account for the development of systems in the next few years, as they should be well optimized and comply with several mandatory requirements that determine whether they are beneficial for the environment and the good progress of society.

In this respect, although wireless power transmission (WPT) technologies are not yet fully optimized, due to the need to find a balance between several factors that decrease overall efficiency, it has become one of the most attractive technologies in the last decade. Therefore, it is important to achieve adequate performance of these systems in terms of reliability, safety and energy efficiency.

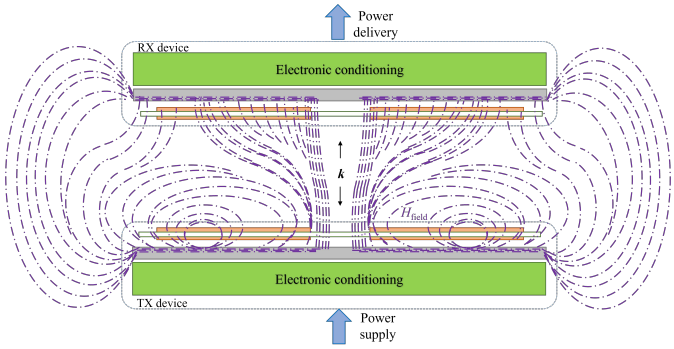

Fig. 1. Wireless power transmission by means of inductive coupling.

Current research in the field of WPT technologies is focused on the optimization of the most promising and pioneering applications. The more usual and popular WPT technology at short-medium distances is the Inductive Power Transmission (IPT) whose key elements are the transmitter and receiver coils, together with the flux concentrator, [1], [2]. Among the most relevant applications at short distances the following can be mentioned: the implementation for induction heating, [3], [4], wireless power supply for medical implants, [5], [6], and static or dynamic charging of electric vehicles, [7], [8], [9].

From a general perspective of technical challenges that battery-powered devices are facing, it can be pointed out that the wireless power transmission offers a new pattern of energization for electric-driven devices, which helps to reduce limitations of cost, heavy weight, low power density, [1]. Interesting road-maps to be followed in the short term are presented in [7], [8], [10], [11], [12], [13].

Some important technical aspects of IPT systems, such as power transfer efficiency, coil design and operation frequency are discussed in [14], and in terms of geometrical aspects such as misalignment or compensation topologies, in [15], [16], [17] are widely analyzed. According to the total efficiency, [18] presents a useful analysis when considering the electronic

Manuscript received August 01, 2022; revised October 24, 2022; accepted January 12, 2023. This work was partly supported by the Spanish MICINN under Projects AEI PID2019-103939RB-I00, PDC2021-120898-I00, TED2021-129274B-I00, CPP2021-008938, ISCIII PI21/00440, co-funded by EU through FEDER and NextGenerationEU/PRTR programs, by the DGA-FSE, and by the BSH Home Appliances Group. (Corresponding author: C. Carretero.)

A. Narvaez and J. Acero are with the Department of Electronic Engineering and Communications, I3A, Universidad de Zaragoza. Maria de Luna 1, 50018 Zaragoza, Spain (e-mail: alexisna@unizar.es, jacero@unizar.es).

C. Carretero and I. Lope are with the Department of Applied Physics, I3A, Universidad de Zaragoza. Pedro Cerbuna, 12, 50009 Zaragoza, Spain (e-mail: ccar@unizar.es, nlope@unizar.es).

power stages of the transmitter side in IPT systems and their associated power losses.

Fig. 1 shows an outline of an inductive power transfer system composed by the transmitter (TX), and receiver (RX). Each side consist of a coil with magnetic flux concentrator and electronic power stage to conditioning the electric power supply or power delivery, respectively. The magnetic flux lines of the time-dependent magnetic field created by the transmitter coil are represented by dashed lines, these flux lines are partially captured in the receiver coil, and in the case of a load connected, wireless power transmission is achieved. The flux concentrator helps to improve wireless power transmission by increasing the coupling factor between the coils, [19].

High-power WPT systems have advanced significantly thanks to efforts to optimize the design of magnetic devices, power electronic stages, control strategies, communication protocols, and other related fields, [20], [21], [22].

Many improvements have been developed through research in loss estimation, [23], [24], [25], optimization of shape and size of the transmitter and receiver coils, [26], [27], testing of different shields to attenuate the stray magnetic field, [28], [29], and also with respect to control techniques to ensure a robust system performance under real operating conditions, [20], [30].

It is worth mentioning that wireless charging systems may offer extra safety benefits than conventional wired systems, for instance, when it comes to powering electronic devices in hostile environments, a wireless power supply may be more reliable because of the hazardous working conditions involved, [31], [32]. Although there are still research gaps to be taken into consideration for a near-flawless performance of the overall system, the authors really consider that they will be mostly solved in the coming years. In this article, the coils of a high-power IPT system are analyzed, because they are the key elements for a properly performance of the whole wireless power transmission system.

This analysis is focused on spiral printed circuit board (PCB) coils with a rectangular cross-sectional area, taking as reference the previous analysis presented in [33], [34], [35], [36], mainly in the field of induction heating. In the first place, the modeling of the losses in coils built on PCBs with litz structure will be described. The losses will be divided into two contributions, associated, on the one hand, with the conduction of the ac current through the tracks and, on the other hand, to the effect produced by the variable magnetic field where the PCB tracks are immersed. The determination of the magnetic fields in the coils will be performed by means of a finite element analysis tool (FEA). The self-inductance of the coils can be also obtained from the FEA simulation results. Next, based on the above procedure, we will proceed to obtain the parameters of the tracks on the printed circuit board optimizing the performance of the coils considering geometrical constraints.

The remainder of the paper is organized as follows. Section II presents the structure of the spiral PCB coils with multitrack litz structure. Section III presents the method to extract the electrical parameters of the coils. Section IV shows the process followed by selecting the most appropriate geometrical parameters to optimize a PCB coil with litz wire structure, regarding the overall energy efficiency of the system as a key parameter. In Section V, some experimental measurements of a prototype with PCB windings for use in an IPT system are presented and compared to simulation results. Finally, in Section VI several conclusions are drawn.

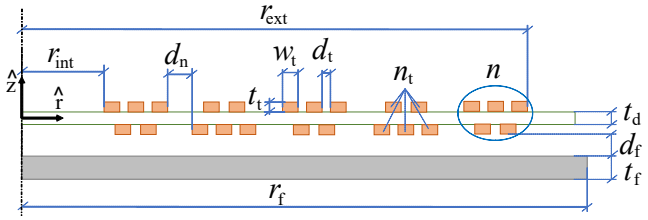

Fig. 2. Geometric parameters of multi-stranded PCB coil.

II. Spiral PCB coils with litz wire structure

The main advantage of using litz wire in coils for inductive power transfer systems operating at medium-high frequencies is the potential reduction on the power losses, [37]. A litz wire structure is composed of several reduced-size strands, isolated and compacted to each other, and the fact that it is a braided wire helps to cancel the voltage induced in any pair of strands, [38]. An analogous structure can be implemented in a spiral PCB coil by splitting each turn in several smaller tracks, and by applying a transposition pattern to the strands, in order to get an equivalence with the conventional litz wire, [39]. The transposition pattern applied to a two-layered PCB coil, by using both the top and bottom layers, ensures that all the strands are equivalent to each other, which means that they are exposed to the same magnetic flux field as well as the voltage induced in any pair of tracks can be canceled out. The effectiveness of using litz wires for power transfer systems can be extended even in the optimization of the shielding, as it appears in [28], with the purpose of attenuating the parasitic magnetic field by reducing the dissipation in this element.

In addition, manufacturing restrictions must be taken into account when designing the spiral PCB coil, such us: minimum clearance between tracks, minimum diameter of vias and drills which are used in the transposition pattern, thickness of the substrate and the copper tracks, etc, although it depends on the limitations of each manufacturer. It is also convenient to minimize the number of changes of layer.

The given nomenclature for the coil parameters is presented in Table I. Fig. 2 shows a typical structure of a two layer multitrack coil composed of $n = 5$ turns and $n_t = 5$ tracks, located over a ferrite plane. It is worth mentioning that an odd number of tracks is recommended to apply an effective litz structure transposition pattern, [39]. Layer changes are made with vias as shown in the Fig. 3, where the transposition pattern is also presented.

The transposition pattern to implement a litz-wire structure in PCB coils is arranged by means of strand displacements and inter-layer connections using vias, [34]. First, the strand is displaced right-to-left in the top layer. When it is at the most extreme location it changes to the bottom layer. At the same

TABLE I
PARAMETER OF PCB COIL GEOMETRY.

Parameter	Symbol
External radius	r_{ext}
Internal radius	r_{int}
Number of turns	n
Number of tracks	n_{t}
Distance between turns	d_{n}
Distance between tracks	d_{t}
Track width	w_{t}
Track thickness	t_{t}
Dielectric thickness	t_{d}
Ferrite distance	d_{f}
Ferrite thickness	t_{f}
Ferrite side half-length	r_{f}

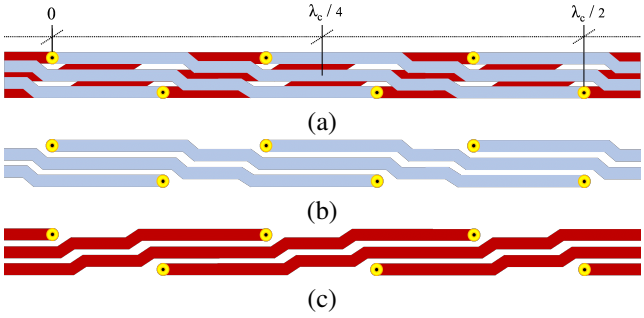

Fig. 3. Transposition pattern applied to obtain a PCB-adapted litz wire structure with $n_{\text{t}} = 5$ tracks: (a) two-layer transposition pattern. Breakdown: (b) top layer transposition pattern, (c) bottom layer transposition pattern.

time, in the bottom layer the opposite occurs, i.e., there is a left-to-right displacement and a down-to-up inter-layer change. The strand is then placed back in the initial layer. It should be noted that the placement of the tracks on the edges of the turns facilitates the routing and results in a better utilization of the copper filling.

In PCB coils with litz wire structure is appropriate to talk about number of layer changes per turn when applying the transposition pattern, [40], a similar metric to twists per unit length in the construction of conventional litz-wires. The optimal number of changes per layer to obtain a null net flux linkage is $n_{\text{ch}} = 2n_{\text{s}}$, but there is a significant reduce of it when every strand occupies more than 2 times (≈ 2.5) every position along the coil.

III. ELECTRICAL PARAMETER MODELING ON PCB COILS

The electrical parameters of the PCB coils are obtained based on the results obtained by finite element simulations. The electrical equivalent of a coil consists of a RL-series circuit. Self-inductance, can be calculated from the FEA tool simulation whereas equivalent resistance requires some additional manipulations of the preceding simulation results.

The series resistance of spiral PCB coils is composed of the conduction and proximity resistances, [2]. The conduction resistance, R_{cond}, includes DC losses and losses associated to the skin effect. The proximity resistance, R_{prox}, considers the power dissipated by the induced current in the conductors by the external varying magnetic field [29]. The total resistance of a coil, R_{w}, can be calculated as follows:

$$R_{\text{w}} = R_{\text{cond}} + R_{\text{prox}}. \tag{1}$$

Conduction resistance, R_{cond}, can be derived from the expression of the conduction resistance, r_{cond}, of a unit length single rectangular cross-section track, as it appears in [39]:

$$r_{\text{cond}} = \frac{1}{w_{\text{t}}\, t_{\text{t}}\, \sigma}\, \Phi_{\text{cond}}\left(w_{\text{t}}, t_{\text{t}}, \delta\right), \tag{2}$$

where w_{t} and t_{t} are the width and thickness of the conductor, respectively, σ is the electrical conductivity of the track, δ is the penetration depth, and the function Φ_{cond} captures the frequency dependence of the skin effects in conductors with a rectangular cross-section. According to [34], the value of the function Φ_{cond} is very close to 1 for optimal geometric parameters of the tracks at typical working frequencies of inductive power transfer systems.

Total conduction resistance, R_{cond}, can be obtained by considering the coil composed of n_{t} equal tracks of MLT length parallel-connected, then:

$$R_{\text{cond}} = \frac{MLT}{n_{\text{t}}} r_{\text{cond}} = \frac{MLT}{n_{\text{t}}} \frac{1}{w_{\text{t}}\, t_{\text{t}}\, \sigma}\, \Phi_{\text{cond}}\left(w_{\text{t}}, t_{\text{t}}, \delta\right), \tag{3}$$

where the mean length turn of a coil with n turns evenly distributed is $MLT = n\pi\left(r_{\text{int}} + r_{\text{ext}}\right)$.

Proximity losses arise from the induced current in a conductor immersed in a variable magnetic field. In cables composed of multiple strands of circular cross-section, the proximity losses are obtained by considering the amplitude of the transverse magnetic field, $\mathbf{H}_0$, generated by the harmonic current of amplitude I_0 driven by the magnetic device. The proximity losses in rectangular cross-section tracks also depends on the amplitude of the transverse magnetic field, $\mathbf{H}_0$, but, on the contrary to round strands, the direction of the field also plays an important role in this kind of losses. Fortunately, the proximity losses in the latter case can be decomposed into two independent contributions associated with the axial, $\mathbf{H}_{0,z}$, and the radial, $\mathbf{H}_{0,r}$, components of the transverse magnetic field, as it is proven in [41]. Proximity losses, $p_{\text{prox},m}$ of a unit length rectangular cross-section track immersed in transverse magnetic field $\mathbf{H}_{0,m}$, where $m = z, r$ corresponds to the axial component, z, or radial component, r, respectively, is given by:

$$p_{\text{prox},m} = \frac{2\pi}{\sigma}\, \Phi_{\text{prox},m}\left(w_{\text{t}}, t_{\text{t}}, \delta\right) |\mathbf{H}_{0,m}|^2, \tag{4}$$

where the function $\Phi_{\text{prox},m}$ accounts for the geometry and frequency dependence of the proximity effects in conductors with a rectangular cross-section and was tabulated and presented in

TABLE II
PARAMETERS VALUES OF THE PCB COIL GEOMETRY.

Parameter	Value
r_{ext}	190 mm
r_{int}	90 mm
n	8
t_{d}	1.55 mm
d_{f}	1 mm
t_{t}	70 μm
d_{n}	250 μm
d_{t}	250 μm
t_{f}	5 mm
r_{f}	201 mm

[34]. It should be noted that $\Phi_{\text{prox},z}$ and $\Phi_{\text{prox},r}$ are the same except exchanging the role of the input geometrical variables w_{t} and t_{t} due to the symmetry of the geometry.

Typically, each section of the track is immersed in a different magnetic field. Considering n_{t} identical tracks, the total proximity losses can be expressed as:

$$P_{\text{prox},m} = n_{\text{t}} \frac{2\pi}{\sigma} \Phi_{\text{prox},m}\left(w_{\text{t}}, t_{\text{t}}, \delta\right) \left\langle |\mathbf{H}_{0,m}|^2 \right\rangle, \tag{5}$$

where the factor $\left\langle |\mathbf{H}_{0,m}|^2 \right\rangle$ is calculated by integrating the square magnetic field along the total length of the track.

Due to the magnetic field arises from the harmonic current of amplitude I_0 driven by coil, it can be useful to normalize the transverse magnetic field amplitude by defining $\overline{\mathbf{H}}_{0,m} = \mathbf{H}_{0,m}/I_0$. Applying the identity $P_{\text{prox},m} = \frac{1}{2} R_{\text{prox},m} I_0^2$, [2], each m component of the proximity resistance can be given by:

$$R_{\text{prox},m} = n_{\text{t}} \frac{4\pi}{\sigma} \Phi_{\text{prox},m}\left(w_{\text{t}}, t_{\text{t}}, \delta\right) \left\langle |\overline{\mathbf{H}}_{0,m}|^2 \right\rangle. \tag{6}$$

Finally, the total coil resistance for a rectangular cross-sectional area spiral PCB coil can be expressed as the addition of the conduction resistance and both components of the proximity resistance:

$$R_{\text{w}} = R_{\text{cond}} + R_{\text{prox},r} + R_{\text{prox},z}. \tag{7}$$

IV. POWER LOSSES OPTIMIZATION

The aforementioned procedure to estimate the equivalent resistance of the PCB coil has been applied to select the optimal track characteristics. Without loss of generality, the IPT system under analysis is composed of equal transmitter and receiver coils. Typical parameters for a vehicle assembly coils has been chosen given by the external coil radius r_{ext}, internal coil radius r_{int}, number of turns n, distance coil to flux concentrator d_{f}, thickness of flux concentrator t_{f}, and side of flux concentrator $2r_{\text{f}}$, listed in the Table II.

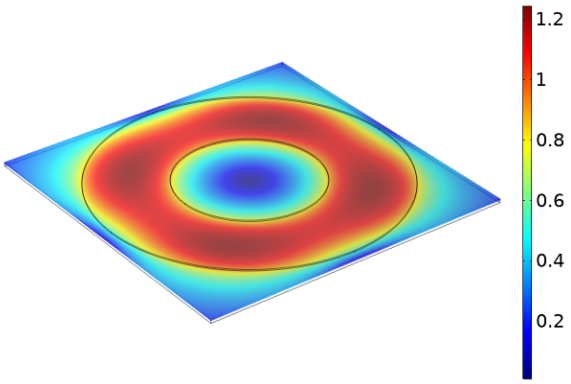

Fig. 4. Magnetic B-field (mT) in the flux concentrator at $I_0 = 1$ A from the FEA electromagnetic simulation of the PCB coil.

The simulation model of one coil of the preceding characteristics was implemented in the COMSOL tool, by applying the homogenization of the internal structure of the tracks, Fig. 4. The coil is modeled in 3D with the parameters:r_{int}, r_{ext}, and a thickness of $t_{\text{coil}} = 2t_{\text{t}} + t_{\text{d}}$. This simple model was constructed in this way, among other reasons, because the meshing of the geometry is simpler compared to a more detailed model, due to the thickness in micrometers of the copper conductor. Winding is modeled as a uniform external current density, acting as the field sources, $\mathbf{J}_{\text{ext}}\left(\mathbf{r}\right) = \frac{nI_{\text{coil}}}{S_{\text{coil}}}$, with S_{coil} the total cross-section area of the coil, [42]. For simplicity I_{coil} is a harmonic current with amplitude of 1 A.

The flux concentrator has a square shape with a side of $2r_{\text{f}}$ and is located at $d_{\text{f}} = 1$ mm under the coil. Ferrite is often used to manufacture flux concentrators, and the material defined in this model has a high permeability of $\mu_r = 2000$.

The induced electromagnetic force in the coil model, V_{coil}, is calculated by integrating the longitudinal electric field, $E_{\parallel}$, in the volume of the coil. It is calculated as:

$$v_{\text{coil}} = -\frac{1}{S_{\text{turn}}} \int_{v_{\text{coil}}} E_{\parallel} dv \tag{8}$$

with the area of each turn is $S_{\text{turn}} = \frac{S_{\text{coil}}}{n}$.

The equivalent impedance of the coil can be calculated by the ratio between the induced EMF in the coil and the current carried by the coil, i.e., $Z_{\text{coil}} = \frac{V_{\text{coil}}}{I_{\text{coil}}}$. So that, the self-inductance of the spiral PCB coil can be obtained as:

$$L_{\text{coil}} = im\left(\frac{Z_{\text{coil}}}{\omega}\right) \tag{9}$$

where the angular frequency is given by: $\omega = 2\pi f$, and f is the frequency in Hz of the current applied to the coil. The real part is null because an ideal coil has been modeled.

The components of the square of the normalized magnetic fields over the volume of the coil are calculated as follows:

$$\left\langle |\overline{\mathbf{H}}_{0,i}|^2 \right\rangle = \frac{1}{S_{\text{coil}}} \int_{V_{\text{coil}}} \left| \frac{\overline{\mathbf{H}}_{0,i}}{I_{\text{coil}}} \right|^2 dv \tag{10}$$

where $i = r$ and z are the radial and axial components,

respectively.

The simulation was carried out in the frequency domain for a single coil at a frequency of 85 kHz. Self-inductance calculated is $L_{\mathrm{w}} = 39.51\ \mu\mathrm{H}$ whereas the components of the square of the normalized magnetic fields over the coil are $\left\langle|\overline{\mathbf{H}}_{0,r}|^2\right\rangle = 11.98\cdot10^3\,1/\mathrm{m}$ and $\left\langle|\overline{\mathbf{H}}_{0,z}|^2\right\rangle = 18.20\cdot10^3\,1/\mathrm{m}$, respectively. The maximum magnetic B-field level in the ferrite is 1.247 mT/A, thus, under typical operational conditions, the importance of the power losses in the flux concentrator is limited.

A. Track number optimization

To get a first approach and overview of the total coil resistance to be obtained, some design parameters have been established such as the minimum distance between tracks or clearance, $d_{\mathrm{t}}^{\min}$, the minimum diameter of the copper ring for the via and drill which is related to the distance between turns, $d_{\mathrm{n}}^{\min}$, and the minimum width of each track, $w_{\mathrm{t}}^{\min}$. All of these parameters depend directly on the thickness of the copper, t_{t}, and manufacturing constraints.

According to the Fig. 2, the following equations can be defined. The range of the width of each turn available in the radial direction can be calculated by subtracting the whole available radial distance minus the distance between turns, as follows:

$$\Delta r_{\mathrm{i}} = \frac{r_{\mathrm{ext}} - r_{\mathrm{int}} - d_{\mathrm{n}}\,(n-1)}{n}. \tag{11}$$

The total number of tracks has to be divided into two layers, so there is necessary to split them in the way:

$$n_{\mathrm{t}} = n_{\mathrm{t,sup}} + n_{\mathrm{t,inf}}. \tag{12}$$

The number of tracks forming a turn should be odd, because the most compact distribution allowing the layer shift of a track must have the space available on the opposite layer. Thus, applying this restriction to the preceding equation, the following conditions can be obtained:

$$n_{\mathrm{t,sup}} = \frac{(n_{\mathrm{t}} \pm 1)}{2} \tag{13}$$

and

$$n_{\mathrm{t,inf}} = \frac{(n_{\mathrm{t}} \mp 1)}{2}, \tag{14}$$

where $n_{\mathrm{t,sup}}$ and $n_{\mathrm{t,inf}}$ are defined as the number of tracks of one turn in the top layer and in the bottom layer, respectively.

The width of each track can be calculated by subtracting the available width per turn minus the whole distance between tracks, and dividing by the maximum number of tracks on both sides, $n_{\mathrm{t},l}^{\max} = (n_{\mathrm{t}}+1)/2$, in such a way:

$$w_{\mathrm{t}} = \frac{\Delta r_{\mathrm{i}} - d_{\mathrm{t}}\left(n_{\mathrm{t},l}^{\max} - 1\right)}{n_{\mathrm{t},l}^{\max}}. \tag{15}$$

By applying (3) and (6) , all the contributions of the total resistance for a conductor with a rectangular cross-section area can be calculated.

TABLE III
PARAMETERS TO MINIMIZE THE TOTAL RESISTANCE.

Parameter	**Value**
n	8
t_{t}	70 μm
d_{n}	250 μm
d_{t}	250 μm
n_{t}	31
w_{t}	533 μm
f	85 kHz
R_{cond}	105.05 mm
$R_{\mathrm{prox},r}$	0.15 mm
$R_{\mathrm{prox},z}$	12.89 mm
R_{w}	118.08 mm

In this analysis, the limitations of the PCB manufacturer have been taken into account to set the specific parameters t_{t}, $d_{\mathrm{n}} = d_{\mathrm{n}}^{\min}$ and $d_{\mathrm{t}} = d_{\mathrm{t}}^{\min}$ of the Table II.

In Fig. 5 are shown the calculated values of the conduction, radial proximity and axial proximity resistances with respect to the number of tracks derived from (3) and (6). These results have been obtained at a frequency of 85 kHz, which is typically used in inductive power transfer systems.

The dependence on the number of tracks of the conduction resistance, R_{cond}, is represented in Fig. 5(a). It should be noted that as the number of tracks increases, the effective cross-section area of each turn is reduced due to the insertion of additional spacing between tracks. On the other hand, in the case of a very small number of tracks, the track width is large enough for the skin effect to increase conduction resistance. Hence, the conduction resistance, R_{cond}, presents a minimum value in the range of 9 to 11 tracks due to the balance between both phenomena. Proximity resistance contribution are also shown in Fig. 5(a). As it can be appreciated, the axial component of the proximity resistance, $R_{\mathrm{prox},z}$, exhibits a strong dependence to the number of tracks because the track width w_{t} determines the relevance of this contribution whereas the radial component of the proximity resistance, $R_{\mathrm{prox},r}$, slightly depends on the number of tracks as well as constitutes a negligible contribution to the total resistance, due to the track thickness t_t is smaller than the width w_t.

The total resistance of the coil, R_{w}, calculated according to (7) is depicted in Fig. 5(b). As it can be observed, the optimal number of tracks to minimize the power losses in the coil is $n_{\mathrm{t}} = 31$ can be easily obtained from the graph. In that case, the characteristics of the coil are presented in the Table III.

V. EXPERIMENTAL RESULTS

A. Prototyping of spiral PCB coils

Fig. 6 shows the PCB coil implemented in a CAD tool. The prototype coils for the transmitter and receiver have

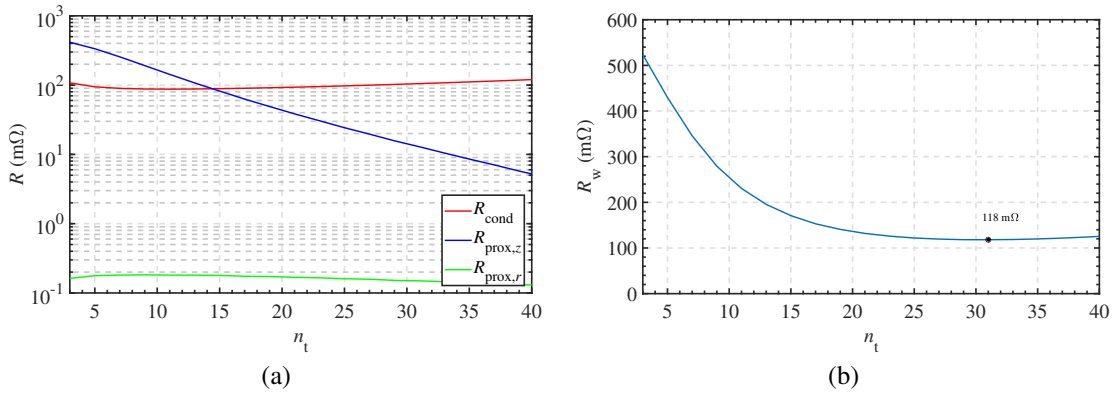

Fig. 5. Geometry optimization of a coil located over a ferrite plane: (a) conduction resistance, R_{cond}, axial component of the proximity resistance,$R_{\text{prox},z}$, and radial component of the proximity resistance, $R_{\text{prox},r}$, (b) total resistance, R_{w}.

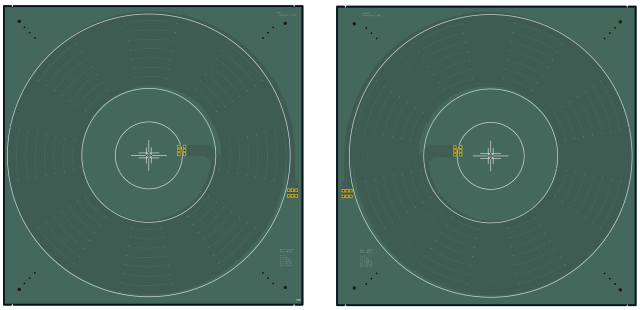

Fig. 6. Spiral PCB coil design, $t_{\text{t}} = 70\ \mu$m , $n_{\text{t}} = 25$: (a) top layer, (b) bottom layer.

been built using the geometric and mathematical description with an automatic method for generating customized PCB coils, the selected copper thickness is $t_{\text{t}} = 70\ \mu$m as in the analysis previously performed. The tool needs values such as outer radius, number of strands, track width, distance between tracks, distance between turns and number of layer changes per turn. The process takes a few minutes and is easy to check if all the manufacturing restrictions are met.

The optimization procedure in the preceding section includes the constraints of the manufacturing process of the tracks. However, considering the need to change the tracks between layers, the constraints imposed for the manufacturing of the vias must also be considered. In the beginning of the design, although the operating temperature was not known, it was assumed that it would increase proportional to the transmitted power. For the sake of simplicity, it can be adequate to consider a minimum track width equal to the minimum diameter of the via ring to avoid lifting of the via pads because of the heat, and thus premature damage to the coil. According to the manufacturer restrictions, the via drill diameter is 250 μm and the annular ring width is 200 μm. Therefore, the minimum width $w_{\text{t}}^{\text{min}} = 650\ \mu$m should be considered in the building process because with $n_{\text{t}} = 31$ only tracks up to $w_{\text{t}} = 533\ \mu$m are feasible. Finally, a lower number of tracks, $n_{\text{t}}^{\text{prot}} = 25$ of width $w_{\text{t}}^{\text{prot}} = 690\ \mu$m were used in the prototype to ensure the distances $d_{\text{t}}^{\text{prot}} = 274\ \mu$m and $d_{\text{n}}^{\text{prot}} = 274\ \mu$m to maintain the inner and outer radii, which are slightly above the

TABLE IV
PARAMETERS OF THE PCB-COIL PROTOTYPE.

Parameter	**Value**
n	8
t_{t}	70 μm
$d_{\text{n}}^{\text{prot}}$	274 μm
$d_{\text{t}}^{\text{prot}}$	274 μm
$n_{\text{t}}^{\text{prot}}$	25
$w_{\text{t}}^{\text{prot}}$	690 μm
f	85 kHz
R_{cond}	100.75 mm
$R_{\text{prox},r}$	0.15 mm
$R_{\text{prox},z}$	22.07 mm
R_{w}	122.98 mm

manufacturer constraints because the spiral turns are built with straight segments. In that configuration, the total resistance is $R_{\text{w}} = 122.98\ \text{m}\Omega$ due to a slight increase in the conduction resistance and a small reduction in the proximity resistances, as shown in Table IV. Regarding the number of changes per turn, they were established to $n_{\text{ch}} = 16$, calculated as $2.5 > n\frac{n_{\text{ch}}}{2}/n_{\text{t}}$. Additionally, each track has been individually attached to the pads of the terminals, in order to preserve the litz structure pattern along all the coil routing.

On the other hand, the ferrite plane was built using ferrite tiles Epcos-TDK N87 of 64 mm x 50.8 mm x 5 mm, with a total length of 385 mm x 406 mm x 5 mm. A distance between the PCB coils and the flux concentrator of 1 mm was established using a mica insulator.

B. LCR experimental measurements

In a first step, the coils have been experimentally characterized by measurements taken with a high precision LCR-meter Agilent E4940AL. The experimental arrangement is shown in Fig. 7(a) for a single PCB-coil. In addition, in Fig.

(a) (b)

Fig. 7. Experimental set-up of small signal characterization: (a) coil over a ferrite plane, (b) transmitter and receiver PCB coils.

7(b) is depicted in detail the inductive power transfer system composed of a receiver coil facing the transmitter pad.

The comparison between experimental measurements and simulation results are represented in the Fig. 8. The proposed model to calculate the coil resistance provides accurate results and a good fit to the experimental data was obtained. As it was expected, at low frequencies the contribution of the conduction resistance, R_{cond}, is dominant, whereas at higher frequencies, the components of the proximity resistances, $R_{\text{prox},r}$ and $R_{\text{prox},z}$, become more important. Regarding the almost frequency-independent self-inductance, $L_{\text{w}} = 39.51\ \mu\text{H}$, as it can be observed, the measured data is in a very good agreement with the preceding value.

Considering the IPT system shown in Fig. 7(b), at the selected distance of 10 cm, the measured mutual coupling inductance $M = 17.65\,\mu\text{H}$ is also in a good agreement to the simulation model value of $18.68\,\mu\text{H}$. The self-inductance value of each PCB coil slightly increases compared to the single coil configuration due to the influence of the flux concentrator on the facing coil, both experimentally measured inductance $L_{\text{coil}} = 42.35\ \mu\text{H}$ and simulated inductance $L_{\text{coil}} = 43.18\ \mu\text{H}$. To avoid adding additional complexity to the analysis, at the selected distance of 10 cm, the influence of the opposite coil and flux concentrator has been neglected. In that arrangement, the coupling factor is $k = 0.42$ at the distance of 10 cm between the transmitter and receiver pads.

C. Measurement at power rating up to 3.3 kW

The basic electronic structure of the inductive power transfer system is shown in Fig. 9. A voltage, V_{in}, is supplied to the input DC bus. The transmitter converter corresponds to a full bridge inverter feeding a series resonant tank composed of the PCB coil and a resonance capacitor. The resonant tank of the receiver is also composed of a PCB coil and a series resonant capacitor. The output voltage of the receiver resonant tank is rectified and slightly filtered by the capacitor C_{f} to fed up the resistive load at voltage V_{out}.

The complete experimental arrangement of the PCB-coil IPT system shown in Fig. 10 comprises the associated electronics, including the DC input power supply, the inverter power-stage, the series resonant tanks, the rectifying and filtering electronics and the output load. The system is operated at fixed switching frequency, $f_{\text{sw}} = 85$ kHz. The resonant tank is designed to obtain a unity-gain output voltage $|G_V| = \left|\frac{V_{\text{out DC}}}{V_{\text{in DC}}}\right| \approx 1$ where minimal load dependence on the receiver side is achieved, [5]. For this purpose, the series compensation capacitors has been calculated by applying:

$$C_i = \frac{1}{\omega_0^2 L_i\,(1 - k_0)} \tag{16}$$

where $i =$ TX or RX, $\omega_0 = 2\pi f_{\text{sw}}$, switching frequency $f_{\text{sw}} = 85\,\text{kHz}$, and the reference coupling factor $k_0 = 0.35$, the value of the resonant capacitors are $C_{\text{TX}} = C_{\text{RX}} = 134.4\,\text{nF}$ but the experimental value of the capacitors are 137.5 nF due to the tolerances of the components,

A resistive power load with a nominal value of R_{L} =4.5 Ω has been connected as the system output load. The control was implemented on a standard development board and managed from MATLAB using a user interface, the open-loop control can adjust the switching frequency, duty cycle and phase between the trigger signals of the full-bridge inverter.

The inverter commutes at a switching frequency of $f_{\text{sw}} = 85$ kHz with a duty cycle of $D = 50\%$, so the way to control the amount of power transferred is by the value of the V_{in}, which is applied directly from a DC power supply. The analysis was carried out on the data captured by a Tektronix DPO7354 oscilloscope.

The maximum power transference tested in the experimental validation was $P_{\text{out}} = 3.3\,\text{kW}$ for a dc input voltage of $V_{\text{in}} = 140$ V. In Fig. 11 are shown the output voltage and current of the transmitter inverter, the voltage in the load, $V_{\text{out}} = 121$ V and the current in the load $I_{\text{out}} = 28$ A. The current density in the receiver coil can be calculated as $J = \frac{I_{\text{rms RX}}}{S_{\text{turn}}} = 25.75\ \text{A/mm}^2$, where $I_{\text{rms RX}} = \frac{\pi}{2\sqrt{2}} I_{\text{out}}$ and $S_{\text{turn}} = n_t w_t t_t$. The high current density achieved can be considered a major advantage of using PCB coils, since convection cooling can be performed more effectively due to the fact that all the strands are isolated by the surrounding air and the board substrate. This is not the case with conventional litz wire where only the external surface of the bundle can dissipate heat.

In order to calculate the power losses dissipated by the IPT system, the following equations have been considered:

$$P_{\text{loss}} = P_{\text{inv}} + P_{C_{\text{TX}}} + P_{L_{\text{TX}}} + P_{L_{\text{RX}}} + P_{C_{\text{RX}}} + P_{\text{rect}}. \tag{17}$$

Inverter losses on the transmitter side can be split into two contributions, the conduction and switching losses, respectively, as it is given as follows:

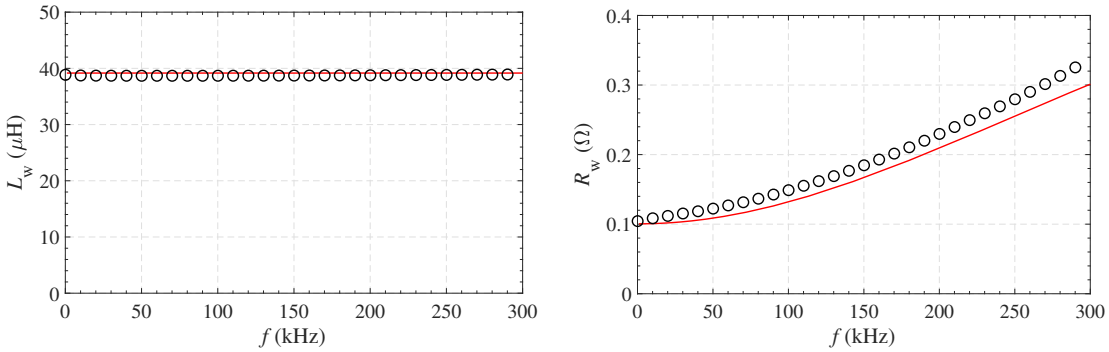

(a) (b)

Fig. 8. Electrical equivalent of the PCB coil (continuous line: simulation data, circular symbols: experimental measurements) for $n_t = 25$, $t_t = 70$ μm: (a) inductance, L_w , (b) resistance, R_w.

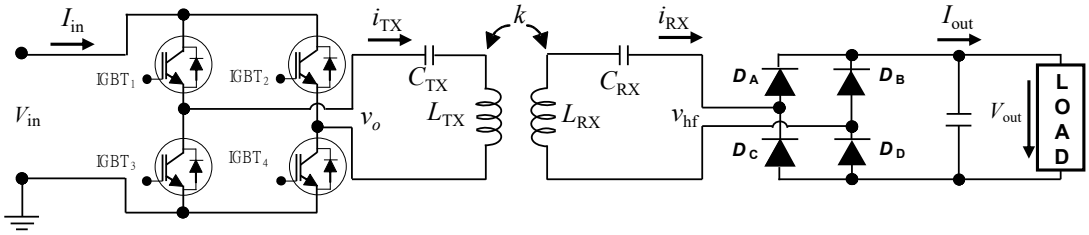

Fig. 9. Schematic of the inductive power transfer system.

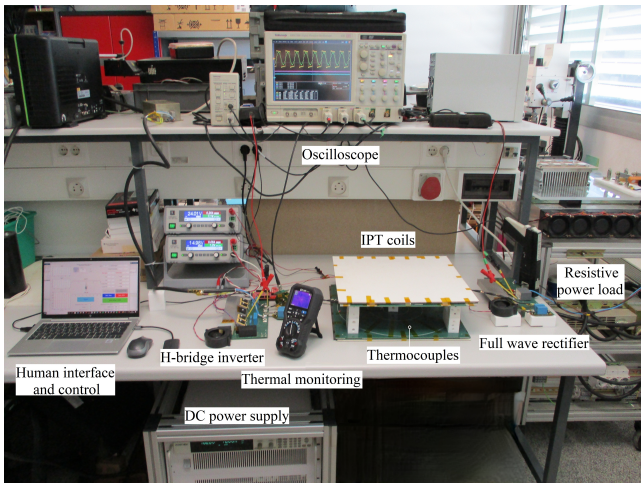

Fig. 10. Experimental set-up of the wireless inductive power transmission system at a distance of 10 cm.

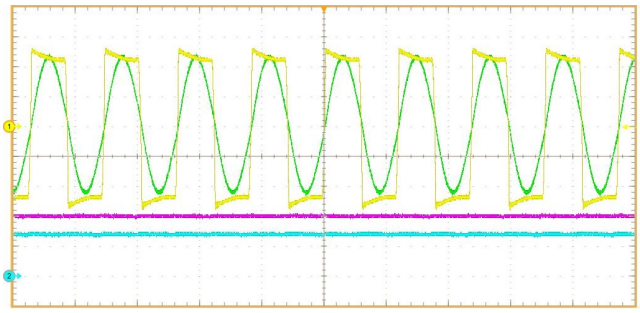

Fig. 11. Experimental waveforms measurements in the IPT system at $P_{out} = 3.3$ kW: output voltage v_o of the transmitter inverter (yellow, 60 V/div); transmitter current i_{TX} (green, 20 A/div); output voltage V_{out} (magenta, 60 V/div) and output current I_{out} (cyan, 20 A/div).

$$P_{inv} = P_{cond} + P_{sw}. \tag{18}$$

Conduction losses of the inverter are calculated in the following way:

$$P_{cond} = 4\, D\, V_{CE}\, I_{IGBTs\ avg}, \tag{19}$$

where $I_{IGBTsavg} = I_{IGBT14\ avg} + I_{IGBT23\ avg}$ is the summation of the average current of each pair of active switching devices. They have the same value if it is assumed that only 2 switching devices are conducting at the same time with a duty cycle $D = 0.50$. However, it can be calculated by means of simulation or by applying: $I_{IGBTs\ avg} = 2\frac{I_{TX,\ peak}}{\pi}$, where $I_{TX,peak}$ is the peak current through the transmitter resonant tank.

Switching losses, which are associated to the dynamic characteristics of the device, are calculated as:

$$P_{sw} = 4 \cdot [0.5\, V_{in}\, I_{cut\text{-}off}\ (t_{on} + t_{off})\ f_{sw}], \tag{20}$$

where V_{in} is the value of the DC input voltage and $I_{cut\text{-}off}$ is the current of the transmitter side at the switching time. Rise and fall time are included in t_{on} and t_{off}, respectively, and f_{sw} is the switching frequency.

The power losses of the receiver rectifier are calculated as:

$$P_{rect} = 2\, V_{fd}\, I_{out}, \tag{21}$$

where V_{fd} is the forward voltage of a single diode and I_{out} is the rectified output current delivered to the power load resistance.

The power losses of the series compensation capacitors are

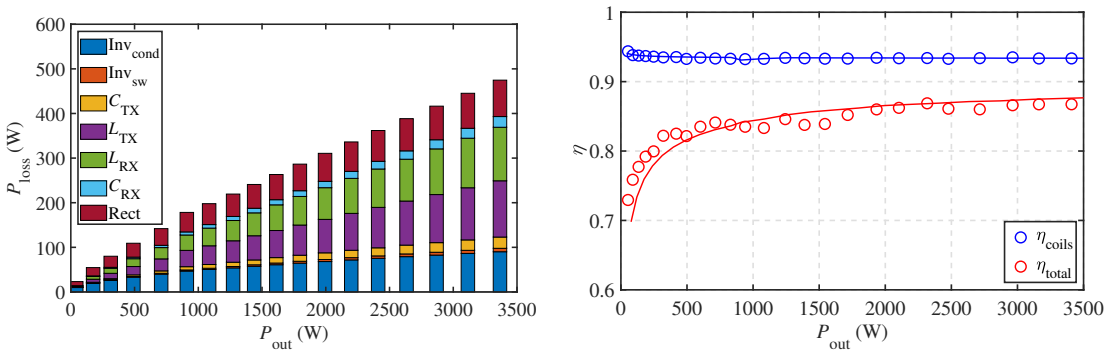

(a) (b)

Fig. 12. Power losses and efficiency of the IPT system: (a) components of the power losses in the IPT system at different output powers, (b) coils and total efficiencies (continuous line: simulation results, circular symbols: measurement data).

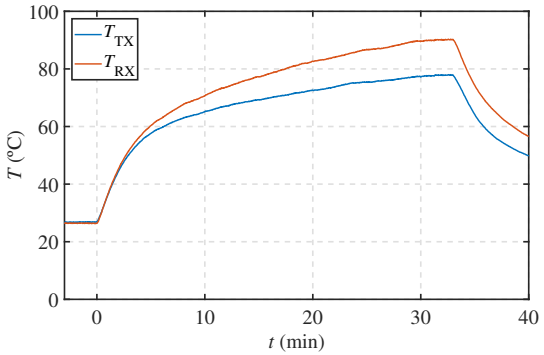

Fig. 13. Transient temperature on the coils with an output power $P_{\text{out}} = 3.3$ kW.

TABLE V
ELECTRICAL FEATURES OF PROTOTYPE DEVICES

Device	**Main features**
IGBTs	$t_{\text{on}} = 30$ ns $t_{\text{off}} = 50$ ns $V_{\text{CE}} = 1.45$ V
Capacitors	$C_{\text{TX}} = C_{\text{RX}} = 137.5$ μF $ESR = 25$ mΩ
PCB Coils	$R_{\text{w}} = 126$ mΩ
Diodes	$V_{\text{fd}} = 1.5$V

calculated taking into account the equivalent series resistance of each capacitor, ESR_{C_i}, at 85 kHz:

$$P_{C_i} = ESR_{C_i} I^2_{\text{rms}_i}, \tag{22}$$

where $i =$ TX or RX represents each side of the IPT system.

In Table V are presented the main electrical features of the standard devices used in the electronic prototyping.

Finally, the power losses on the PCB coils are obtained from the coil resistance, R_{w}, as it performed in the following expression:

$$P_{\text{w}_i} = R_{\text{w}_i} I^2_{\text{rms}_i}. \tag{23}$$

As far as both resonant tanks are identical, the losses depend mainly on the RMS current of each resonant tank.

The overall efficiency of the inductive power transfer system can be calculated as:

$$\eta_{\text{total}} = \frac{P_{\text{out}}}{P_{\text{in}}} = \frac{P_{\text{out}}}{P_{\text{loss}} + P_{\text{out}}}. \tag{24}$$

The efficiency of the coils can be expressed by:

$$\eta_{\text{coils}} = \frac{P_{\text{RX}}}{P_{\text{TX}}} = \frac{P_{C_{\text{RX}}} + P_{\text{rect}} + P_{\text{out}}}{P_{\text{w}_{\text{TX}}} + P_{\text{w}_{\text{RX}}} + P_{C_{\text{RX}}} + P_{\text{rect}} + P_{\text{out}}}, \tag{25}$$

where P_{TX} and P_{RX} are the input power to the transmitter coil and the output power of the receiver coil, respectively.

Fig. 12(a) represents the breakdown of energy losses calculated from the preceding expressions for different levels of power delivered to the load. As it can be seen, losses on the power electronics are more relevant for output power below 1 kW, but as the output power increases, coil losses gain importance. On the other hand, the Fig. 12(b) presents the experimental and simulation results of total and coils efficiencies, as were defined in (24) and (25), respectively. The coils efficiency is $\eta_{\text{coils}} = 93\%$ and the total efficiency is around $\eta_{\text{total}} = 88\%$ for an output power of $P_{\text{out}} = 3.3$ kW. A good agreement between the calculated and experimentally measured efficiencies is observed.

D. Thermal performance of the IPT system

Temperature probes have been placed at transmitter and receiver coils to check the thermal performance of the PCB coils. The system was monitored for an output power $P_{\text{out}} = 3.3$kW for more than half an hour. The results obtained are presented in Fig. 13. As it can be seen, the temperature of the coils always have operated at a safe operating point for the PCB material significantly below 85°C.

The wireless power transmission was performed for a total of 33 minutes, and according to the figure presented, the system reached thermal stability in about 29 minutes of operation. After reaching a steady-state operation, the system was deactivated, and the cooling curve followed by the coils can be observed in the figure since minute 33, approximately.

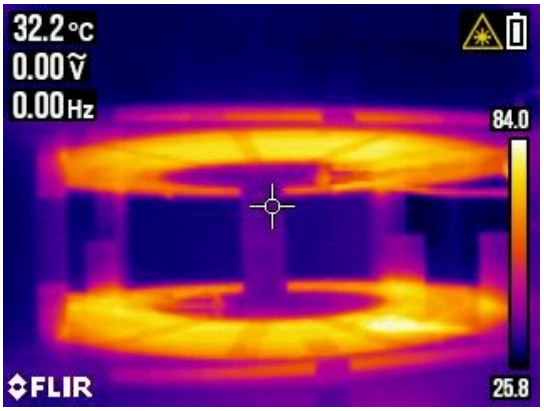

Fig. 14. Thermal camera capture of the transmitter and receiver coils after 30 minutes at $P_{\text{out}} = 3.3\,\text{kW}$.

In Fig. 14 is depicted the thermal profile captured with a infrared camera after 30 minutes of operation delivering an output power $P_{\text{out}} = 3.3\,\text{kW}$. As it can be seen, the system has no hot spots that could lead to system failures.

VI. Conclusion

In this work, an optimization method has been developed to obtain the characteristics of the tracks for PCB-coils of inductive power transfer systems applying litz-wire transposition pattern to equalize the total resistance of the tracks. A mixed-calculation strategy is adopted by the combination of finite element simulations and the use of resistance formulas for the PCB tracks. From the simulation, it is possible to obtain the mean square field in the coil, which constitutes an essential parameter for calculating track losses. In the coil optimization procedure, it is essential to consider the manufacturing constraints.

The presented design methodology was firstly validated by means of the small-signal impedance measurement of the physical prototype. The successful performance of the PCB coils under real working conditions were also validated by means of experimental measurements and compared to simulation results. The thermal behavior of the IPT system was tested for more than half an hour at an output power around 3.3 kW. Due to the optimized series resistance of the coil, the coil power losses have been fairly minimized. The temperature variation of the coils with respect to the ambient temperature reaches up to 60°C. The combined efficiency of the coils was close to 93% and the total efficiency is 88% at maximum output power. This study do emphasize the suitability of optimized spiral PCB coils with litz structure for IPT systems at this power range. It might be of great interest to implement the developed coils in a real IPT system by exchanging the conventional coils for the ones developed in this study, in order to obtain a practical low-profile arrangement.

References

[1] Z. Zhang, H. Pang, A. Georgiadis, and C. Cecati, "Wireless Power Transfer - An Overview," *IEEE Transactions on Industrial Electronics*, vol. 66, no. 2, pp. 1044–1058, 2019.

[2] C. Carretero, "Coupling Power Losses in Inductive Power Transfer Systems With Litz-Wire Coils," *IEEE Transactions on Industrial Electronics*, vol. 64, no. 6, pp. 4474–4482, 2017.

[3] O. Lucia, J. Acero, C. Carretero, and J. Burdio, "Induction Heating Appliances," *IEEE Industrial Electronics Magazine*, vol. 1, no. September, pp. 35–47, 2013.

[4] J. Serrano, I. Lope, and J. Acero, "Nonplanar Overlapped Inductors Applied to Domestic Induction Heating Appliances," *IEEE Transactions on Industrial Electronics*, vol. 66, no. 9, pp. 6916–6924, 2019.

[5] O. Knecht and J. W. Kolar, "Performance Evaluation of Series-Compensated IPT Systems for Transcutaneous Energy Transfer," *IEEE Transactions on Power Electronics*, vol. 34, no. 1, pp. 438–451, 2018.

[6] T. Campi, S. Cruciani, F. Maradei, A. Montalto, F. Musumeci, and M. Feliziani, "Centralized High Power Supply System for Implanted Medical Devices Using Wireless Power Transfer Technology," *IEEE Transactions on Medical Robotics and Bionics*, vol. 3, no. 4, pp. 992–1001, 2021.

[7] A. Ahmad, M. S. Alam, and R. Chabaan, "A Comprehensive Review of Wireless Charging Technologies for Electric Vehicles," *IEEE Transactions on Transportation Electrification*, vol. 4, no. 1, pp. 38–63, 2017.

[8] D. Patil, M. K. McDonough, J. M. Miller, B. Fahimi, and P. T. Balsara, "Wireless Power Transfer for Vehicular Applications: Overview and Challenges," *IEEE Transactions on Transportation Electrification*, vol. 4, no. 1, pp. 3–37, 2017.

[9] S. Chatterjee, A. Iyer, C. Bharatiraja, I. Vaghasia, and V. Rajesh, "Design Optimisation for an Efficient Wireless Power Transfer System for Electric Vehicles," *Energy Procedia*, vol. 117, pp. 1015–1023, 2017.

[10] H. Feng, R. Tavakoli, O. C. Onar, and Z. Pantic, "Advances in High-Power Wireless Charging Systems: Overview and Design Considerations," *IEEE Transactions on Transportation Electrification*, vol. 6, no. 3, pp. 886–919, 2020.

[11] H. T. Nguyen, J. Y. Alsawalhi, K. A. Hosani, A. S. Al-Sumaiti, K. A. A. Jaafari, Y. J. Byon, and M. S. E. Moursi, "Review Map of Comparative Designs for Wireless High-Power Transfer Systems in EV Applications: Maximum Efficiency, ZPA, and CC/CV Modes at Fixed Resonance Frequency Independent from Coupling Coefficient," *IEEE Transactions on Power Electronics*, vol. 37, no. 4, pp. 4857–4876, 2022.

[12] Y. Yao, P. Sun, X. Liu, Y. Wang, and D. Xu, "Simultaneous Wireless Power and Data Transfer: A Comprehensive Review," *IEEE Transactions on Power Electronics*, vol. 37, no. 3, pp. 3650–3667, 2022.

[13] A. Mahesh, B. Chokkalingam, and L. Mihet-Popa, "Inductive Wireless Power Transfer Charging for Electric Vehicles-A Review," *IEEE Access*, vol. 9, pp. 137 667–137 713, 2021.

[14] J. Acero, I. Lope, C. Carretero, and J. M. Burdio, "Analysis of Winding Loss and Optimization of Inductive Power Transfer Coils," *IEEE International Symposium on Industrial Electronics*, vol. 2020-June, pp. 1435–1441, 2020.

[15] D. Maier, W. Ye, and N. Parspour, "Contactless Energy Transfer-Analytical Calculation of the Coil Systems' Efficiencies for Different Topologies," *2021 IEEE PELS Workshop on Emerging Technologies: Wireless Power Transfer, WoW 2021*, pp. 1–5, 2021.

[16] J. Mai, X. Zeng, Y. Yao, Y. Wang, and D. Xu, "Improved Winding and Compensation Methods for the Multi-layer Coil in IPT System," *IEEE Transactions on Industrial Electronics*, vol. 0046, no. c, 2021.

[17] Z. She, S. Chen, Y. Chen, Y. Zhang, H. Li, and Y. Tang, "Efficiency Analysis of LCC-S and S-S Inductive Power Transfer Considering Switching Device and Component Losses," *2020 IEEE 9th International Power Electronics and Motion Control Conference, IPEMC 2020 ECCE Asia*, pp. 2956–2960, 2020.

[18] R. Okada, R. Ota, and N. Hoshi, "IPT System Efficiency Improvement Considering Loss Characteristics of Inverter and Resonant Circuit," *2020 IEEE 9th International Power Electronics and Motion Control Conference, IPEMC 2020 ECCE Asia*, pp. 753–760, 2020.

[19] C. Carretero, I. Lope, and J. Acero, "Magnetizable Concrete Flux Concentrators for Wireless Inductive Power Transfer Applications," *IEEE Journal of Emerging and Selected Topics in Power Electronics*, vol. 8, no. 3, pp. 2696–2706, 2020.

[20] F. Xu, S. C. Wong, and C. K. Tse, "Overall Loss Compensation and Optimization Control in Single-Stage Inductive Power Transfer Converter Delivering Constant Power," *IEEE Transactions on Power Electronics*, vol. 37, no. 1, pp. 1146–1158, 2022.

[21] J. Zhang, Z. He, A. Luo, Y. Liu, G. Hu, X. Feng, and L. Wang, "Total Harmonic Distortion and Output Current Optimization Method of Inductive Power Transfer System for Power Loss Reduction," *IEEE Access*, vol. 8, pp. 4724–4736, 2020.

[22] R. Tanzania, F. H. Choo, and L. Siek, "Design of WPT Coils to Minimize AC Resistance and Capacitor Stress Applied to SS-topology," *IECON*

2015 - 41st Annual Conference of the IEEE Industrial Electronics Society, pp. 118–122, 2015.
[23] B. Nawaz, C. Som, and C. Schaffelhofer, "A Novel Method to Calculate the Efficiency of a Wireless Power Transfer System Using Modified Ferreira's/Dowell's Method," *2020 IEEE Applied Power Electronics Conference and Exposition (APEC)*, pp. 3132–3139, 2020.
[24] G. R. Kalra, M. G. S. Pearce, S. Kim, D. J. Thrimawithana, and G. A. Covic, "A Power Loss Measurement Technique for Inductive Power Transfer Magnetic Couplers," *IEEE Journal of Emerging and Selected Topics in Industrial Electronics*, vol. 1, no. 2, pp. 113–122, 2020.
[25] D. Chen, L. Wang, C. Liao, and Y. Guo, "The Power Loss Analysis for Resonant Wireless Power Transfer," *IEEE Transportation Electrification Conference and Expo, ITEC Asia-Pacific 2014 - Conference Proceedings*, pp. 7–10, 2014.
[26] J. Cho, J. Sun, H. Kim, J. Fan, Y. Lu, and S. Pan, "Coil Design for 100 KHz and 6.78 MHz WPT System: Litz and Solid Wires and Winding Methods," *IEEE International Symposium on Electromagnetic Compatibility*, pp. 803–806, 2017.
[27] S. Mehri, A. C. Ammari, J. B. H. Slama, and M. Sawan, "Design Optimization of Multiple-Layer PSCs with Minimal Losses for Efficient and Robust Inductive Wireless Power Transfer," *IEEE Access*, vol. 6, pp. 31 924–31 934, 2018.
[28] M. Lu and K. D. Ngo, "Circuit Models and Fast Optimization of Litz Shield for Inductive-Power-Transfer Coils," *IEEE Transactions on Power Electronics*, vol. 34, no. 5, pp. 4678–4688, 2019.
[29] ——, "Analytical Calculation of Proximity-Effect Resistance for Planar Coil with Litz Wire and Ferrite Plate in Inductive Power Transfer," *IEEE Transactions on Industry Applications*, vol. 55, no. 3, pp. 2984–2991, 2019.
[30] M. Kamat and M. Patt, "Active Phase Shifting Method for Different Resonant Converter Configurations in Inductive Power Transfer (IPT) Systems," *2019 21st European Conference on Power Electronics and Applications, EPE 2019 ECCE Europe*, pp. 1–10, 2019.
[31] D. Axinte, X. Dong, D. Palmer, A. Rushworth, S. C. Guzman, A. Olarra, I. Arizaga, E. Gomez-Acedo, K. Txoperena, K. Pfeiffer, F. Messmer, M. Gruhler, and J. Kell, "MiRoR - Miniaturized Robotic Systems for Holistic In-Situ Repair and Maintenance Works in Restrained and Hazardous Environments," *IEEE/ASME Transactions on Mechatronics*, vol. 23, no. 2, pp. 978–981, 2018.
[32] J. D. Lopez-Cardona, C. Vazquez, D. S. Montero, and P. C. Lallana, "Remote Optical Powering Using Fiber Optics in Hazardous Environments," *Journal of Lightwave Technology*, vol. 36, no. 3, pp. 748–754, 2018.
[33] J. Serrano, I. Lope, J. Acero, C. Carretero, J. M. Burdío, and R. Alonso, "Design and Optimization of Small Inductors on Extra-thin PCB for Flexible Cooking Surfaces," *IEEE Transactions on Industry Applications*, vol. 53, no. 1, pp. 371–379, 2017.
[34] I. Lope, C. Carretero, J. Acero, R. Alonso, and J. M. Burdio, "Frequency-dependent Resistance of Planar Coils in Printed Circuit Board with Litz Structure," *IEEE Transactions on Magnetics*, vol. 50, no. 12, pp. 1–9, 2014.
[35] S. Mehri, A. C. Ammari, J. Slama, and M. Sawan, "Minimizing Printed Spiral Coil Losses for Inductive Link Wireless Power Transfer," *2016 IEEE Wireless Power Transfer Conference, WPTC 2016*, pp. 41–44, 2016.
[36] J. Serrano, J. Acero, I. Lope, C. Carretero, and J. M. Burdio, "A Flexible Cooking Zone Composed of Partially Overlapped Inductors," *IEEE Transactions on Industrial Electronics*, vol. 65, no. 10, pp. 7762–7771, 2018.
[37] I. Lope, C. Carretero, J. Acero, J. M. Burdío, and R. Alonso, "Practical Issues when Calculating AC Losses for Magnetic Devices in PCB Implementations," *Conference Proceedings - IEEE Applied Power Electronics Conference and Exposition - APEC*, pp. 1017–1022, 2012.
[38] J. Serrano, I. Lope, J. Acero, C. Carretero, and J. M. Burdio, "Mathematical Description of PCB-adapted Litz Wire Geometry for Automated Layout Generation of WPT Coils," *Proceedings IECON 2017 - 43rd Annual Conference of the IEEE Industrial Electronics Society*, vol. 2017-Janua, no. 1, pp. 6955–6960, 2017.
[39] I. Lope, J. Acero, J. M. Burdio, C. Carretero, and R. Alonso, "Design and Implementation of PCB Inductors with Litz-wire Structure for Conventional-size Large-signal Domestic Induction Heating Applications," *IEEE Transactions on Industry Applications*, vol. 51, no. 3, pp. 2434–2442, 2015.
[40] I. Lope, C. Carretero, J. Acero, J. Serrano, and J. M. Burdío, "Equivalence Among Strands in PCB Litz-wire Inductors Applied to Domestic Induction Heating," *International Journal of Applied Electromagnetics and Mechanics*, vol. 53, pp. S129–S137, 2017.
[41] I. Lope, C. Carretero, J. Acero, R. Alonso, and J. Burdio, "AC Power Losses Model for Planar Windings With Rectangular Cross-Sectional Conductors," *IEEE Transactions on Power Electronics*, vol. 29, no. 1, pp. 23–28, 2014.
[42] C. Carretero, O. Lucia, J. Acero, R. Alonso, and J. Burdio, "Frequency-dependent Modelling of Domestic Induction Heating Systems using Numerical Methods for Accurate Time-domain Simulation," *IET Power Electronics*, vol. 5, no. 8, pp. 1291–1297, 2012.

Alexis Narvaez (Graduate Student Member, IEEE) received the B.Eng and M.Eng. degrees in electrical engineering from the University of Zaragoza in 2018 and 2019, respectively, where he is currently working toward the Ph.D. degree with the Department of Electronic Engineering and Communications. His main research interests include electromagnetic modeling of magnetic devices, and power electronics and control applied to inductive coupled transmission systems. He is a member of the Power Electronics and Microelectronics Group (GEPM), Instituto de Investigacion en Ingenieria de Aragon (I3A).

Claudio Carretero (Senior Member, IEEE) received the M.Sc. degree in physics, the M.Eng. degree in electrical engineering and the Ph.D. degree in electrical engineering from the University of Zaragoza, in 1998, 2002 and 2010, respectively. He is currently Associate Professor at the Department of Applied Physics, University of Zaragoza. His research interests include induction heating applications and electromagnetic modeling of inductive systems. He is a member of the Instituto de Investigacion en Ingenieria de Aragon (I3A).

Ignacio Lope (Member, IEEE) received the M.Eng. degree in electrical engineering and the Ph.D. degree in power electronics from Universidad de Zaragoza, Zaragoza, Spain, in 2010 and 2015, respectively. He has been working from 2015 to 2022 in BSH Home Appliances, Zaragoza, where he was involved in several projects focusing on developing domestic induction heating appliances. He is currently Assistant Professor of Electromagnetism with the Department of Applied Physics, Universidad de Zaragoza. His current research interests include electromagnetic modeling of inductive coupled contactless energy transfer systems and loss modeling of magnetic devices. Dr. Lope is a member of the Instituto de Investigacion en Ingenieria de Aragon (I3A).

Jesus Acero (Senior Member, IEEE) received the M.Eng. and Ph.D. degrees in electrical engineering from the University of Zaragoza, Zaragoza, Spain, in 1992 and 2005, respectively. From 1992 to 2000, he worked on several industry projects, especially focused on custom power supplies for research laboratories. Since 2000 he has been with the Department of Electronic Engineering and Communications at the University of Zaragoza, Spain, where he is currently a Professor. His main research interests include resonant converters for induction heating applications, inductive-type load modeling, and electromagnetic modeling. Prof. Acero is a Member of the IEEE Power Electronics, Industrial Electronics and Magnetics Societies. Prof. Acero is also a member of the Instituto de Investigacion en Ingenieria de Aragon (I3A).